Magnetic vortices in nanowires with transverse easy axis

Laurent Vila,[1,2] Michaël Darques,[1] Armando Encinas,[1,3] Ursula Ebels,[2] Jean-Marie George,[4] Giancarlo Faini,[5] André Thiaville,[6] and Luc Piraux[1]

[1]*Unité PCPM, Université Catholique de Louvain, 1348 Louvain-la-Neuve, Belgium*

[2]*CEA, INAC, 17 Avenue des Martyrs, 38054 Grenoble, France*

[3]*Instituto de Física, Universidad Autonoma de San Luis Potosi, San Luis Potosi, Mexico*

[4]*Unité Mixte de Physique CNRS/Thales, Université Paris XI Orsay, RD128, 91767 Palaiseau, France*

[5]*Phynano team, Laboratoire de Photonique et de Nanostructures, CNRS, Route de Nozay, 91960 Marcoussis, France*

[6]*Laboratoire de Physique des Solides, Université Paris XI Orsay, 91405 Orsay, France*

(Received 16 March 2009; published 22 May 2009)

We present magnetotransport measurements as well as micromagnetic simulations of magnetization reversal in magnetic nanowires having strong transverse magnetocrystalline anisotropy. The interplay between exchange, demagnetizing, and magnetocrystalline energies gives rise to a micromagnetic configuration involving vortices with alternative chirality along the wire. Despite the complexity of the field angle-dependent magnetization reversal process, a very good agreement is obtained between experiments and simulations. This provides evidence that the reported magnetization process appears generally in nanowires with strong transverse magnetocrystalline anisotropy. Moreover an analytical expression is established for the angular dependency of the core switching field. The simulations indicate the occurrence of Bloch points during the core reversal.

DOI: 10.1103/PhysRevB.79.172410 PACS number(s): 72.15.Eb, 75.47.−m, 75.60.Jk, 75.75.+a

Magnetism at a small scale addresses both important fundamental and application aspects. Shrinking the dimensions of magnetic systems down to the typical magnetic length scales is a novel opportunity to get insights into nanomagnetism. Also applications are likely to take advantage of geometrically confined magnetic states, such as single domains, for data storage or localized magnetic field sources. Nanowires are model objects for such purposes. However, focusing on small and single nanomagnets is still challenging. A powerful tool in such concern is to combine magnetotransport measurements and micromagnetic simulations.

Using nanoporous templates,[1,2] it is possible to grow well-defined cylindrical ferromagnetic nanowires with diameters as small as 20 nm and extremely large aspect ratios (up to a thousand). Therefore, being quasi-one-dimensional systems, they can be compared with analytical solutions of coherent reversal such as Stoner-Wohlfarth[3] and curling models.[4] For Ni, Fe, and their alloys, the nanowire properties are dominated by the shape anisotropy[5] and the behavior is now well understood. It has been established that the reversal of the magnetization is governed by the nucleation of a reverse domain at the wire extremities and its subsequent propagation along the wire.[6–8]

For Co nanowires, a strong transverse magnetocrystalline anisotropy (MCA) can be introduced, leading to a more complicated behavior.[7,9,10] Under certain electroplating conditions Co grows in the hexagonal phase, giving rise to a strong transverse MCA, of the order of magnitude of the shape anisotropy.[11,12] In that case, the high degree of symmetry is broken due to the interplay between shape and magnetocrystalline anisotropies. In previous studies on such nanowires, magnetic force microscopy (MFM) observations and anisotropic magnetoresistance (AMR) measurements have shown that, at remanence, states with strong out of the wire-axis component can be present.[10,13,14] One concern is the transition between single domain, domains with transverse magnetization, and flux-closure state along the wire.[10,13,15,16] The latter has drawn a lot of interest in flat-magnetic elements, especially with the singularity arising from magnetic vortices. More recently, there is growing interest in ultrafast vortex-core reversal through the propagation of a Bloch point.[17,18]

In this Brief Report we focus on the magnetic properties of high aspect ratio (60 nm diameter and several μm long) nanowires with a strong perpendicular to the wire-axis anisotropy. Important results on the magnetization-reversal mechanism come from the angular dependency of the AMR measured on a segment of a long Co nanowire by a multiprobe technique[14,19] and its understanding in light of micromagnetic simulations (Fig. 1). The magnetization reversal involves vortex states that provide an opportunity to precisely control the nanowire switching field. The micromagnetic simulations show a direct core reversal through the propagation of a Bloch point.

The multiple contacts along the single nanowire have been realized by electron-beam lithography as detailed elsewhere.[19] For such a purpose the nanowires are extracted from the nanoporous media and spread over a silicon substrate. The OOMMF software[20] has been used for the micromagnetic simulation. We have shown in a previous study that such Co nanowires grow in hexagonal phase and that for the present growth conditions the so-called c axis of the grains can be either parallel, perpendicular, or at an angle respect to the wire axis.[14] The typical grain size was found to be around 1 μm.

The angular dependence of the AMR presented in Fig. 1(a) can be understood in the light of the structural properties. The high-(low-)resistance state indicates that the micromagnetic configuration has a large magnetization component parallel (perpendicular) to wire axis. At remanence, the system is in a low-resistance state close to the value obtained in the perpendicular-saturated state. This corresponds to a mag-

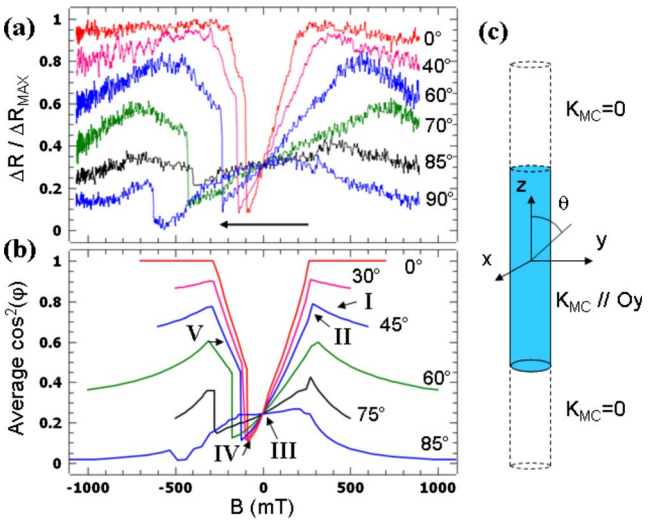

FIG. 1. (Color online) (a) Experimental and (b) calculated angular dependency of the AMR. The field direction is indicated by the arrow. The angle θ between the applied field and the wire axis is indicated in the figures. In (b), I, II, III, IV, and V refer to the magnetic sketches depicted in Figs. 2 and 3. (c) Schematic of the simulated system with the central grain having a MCA along (Oy).

netic state with a strong component of the magnetization lying in the perpendicular to the wire direction. This is unusual in the case of high aspect-ratio wires where usually high resistance states are found at remanence. Moreover, this is independent of the magnetic history, showing that the system always goes to a very similar magnetic state whatever the initial saturation direction. Also, in the parallel direction, the reversal starts well before the field reversal, corresponding to the decrease in the resistance. This suggests that the measurements were performed on a grain having a strong perpendicular to the wire MCA. The MCA forces the magnetization to be mostly perpendicular to the wire at remanence, corresponding to the fundamental state.

In order to understand this unusual behavior, micromagnetic simulations were performed considering a wire having a perpendicular MCA. The parameter values are

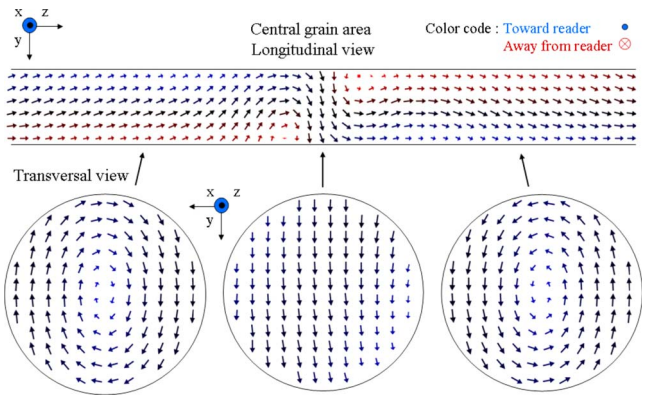

FIG. 2. (Color online) Micromagnetic configuration at remanence inside the central grain. Top: longitudinal cut through the center and bottom: three transversal views at the positions indicated by the arrows (the out of the plane component is color coded).

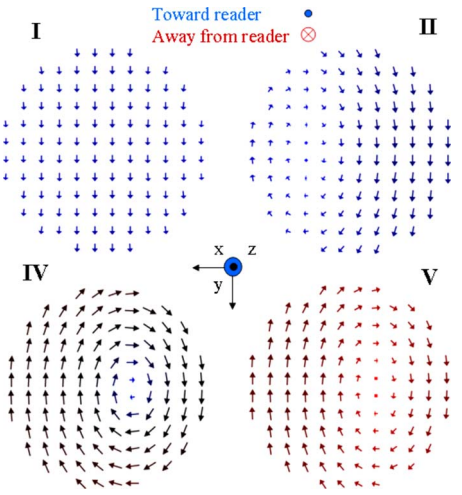

FIG. 3. (Color online) Micromagnetic sketches of the reversal process for the general case $\theta < 75°$ at the steps indicated in Fig. 1(b) (see the color code for the out of the plane direction): (I) after saturation, (II) after nucleation (the remanent state (III) is displayed in Fig. 2), (IV) before and (V) after core reversal.

1400×10^3 A/m, 2×10^{11} J/m, and 4.5×10^5 J/m^3 for the magnetization at saturation (M_s), the exchange constant, and the magnetocrystalline energy, respectively. The geometry is described in the schematic of Fig. 1(c) (other geometries have been also put to test and show similar results). The 60-nm-diameter wire consists of three 500-nm-long grains. Only the central grain has a MCA axis oriented along (Oy), the two surrounding grains keep away the wire ends that are strong sources of demagnetizing field. The MC axis of the central grain is oriented perpendicular to the wire axis, as deduced from the AMR measurements. The field is applied in the plane defined by (yOz), θ being the angle between the applied field and the wire axis (Oz). The cell size is 5 nm along the wire axis and 2.5 nm along (Ox) and (Oy) axes. The application of successive discrete field steps simulates the magnetic cycle. At each applied field, the AMR value in the central grain area is estimated as the average of $\cos^2(\phi)$ with ϕ the angle between the local magnetization and the wire axis.[21] The angular dependency of the calculated AMR is shown in Fig. 1(b).

A very good agreement is found between the experiment and the simulations. Indeed, the jumps corresponding to the reversal as well as the changes in the slope of the curves at positive and negative field values are reproduced. The remanent state corresponds also to a low-resistance state. While close to the parallel direction the resistance is strongly modified during the reversal, the changes in resistance are much less pronounced close to the perpendicular direction. Thus the micromagnetic configurations obtained in the simulation are well representative of the experimental situation.

Figure 2 depicts the micromagnetic configuration obtained in the central grain area at remanence. Independently of the magnetic history, the remanent state involves two magnetic vortices along the wire with alternate chirality. Compared to a single-domain transverse state, a vortex reduces the demagnetizing energy at the cost of exchange energy. It should be noted that the vortex is not fully symmetric

since the MCA induces a deformation of the close loop of the magnetization vector along (Oy), source of stray field. The two vortices along the grain length are of opposite chirality (clockwise and counter clockwise) in order to further lower the demagnetizing energy. In the transition region between the two vortices (domain wall), the cores of the two vortices are expelled at the surface of the wire, in opposite directions. In the middle plane, all spins are perpendicular to the wire, along the MCA direction.

The magnetization maps for the 45° cycle are shown in Fig. 3 where I, II, IV, and V refer to the corresponding resistance values in the AMR curve in Fig. 1(b). It is the same plane as shown in the left-transversal view of Fig. 2 of the central grain area. This well represents the general case (i.e., $\theta<75°$) of the magnetization reversal. In I, the system is in a saturated single-domain state oriented at 45°. When the field value is decreased the magnetization starts to relax toward the wire axis (corresponding to the increase in resistance). Reducing further the field, the magnetization of adjacent spins splits, allowing the creation of the circular path required for the vortex nucleation (II). At that point the magnetization is mostly along the wire axis. The circular path appears at the wire border as it is found for dots. Decreasing the field value down to zero lets the spins rotate transverse to the wire axis, whereas the vortex cores move toward the wire axis (the resistance is decreasing). In III, the system is at remanence and the vortex core is located at the wire center as in Fig. 2. The vortex core is oriented along the wire axis and points toward the saturation direction.

When the field is reversed the vortex core starts to move toward the other wire border, opposite to its nucleation point (IV). This is also observed for magnetic vortices in dots. The volume parallel to the field direction increases at the cost of the volume antiparallel to it, making the vortex core move from one side to the other. There is a reduction of the vortex-core dimension since it is antiparallel to the axial-field component. When the field is strong enough, the situation with the vortex core pointing in the opposite to the field direction is not possible any more and the core reverses. After the reversal (V), the magnetization is mostly pointing along the z direction with still the circular path similar to the curling state. The two domains have again opposite chirality. The reversal corresponds to an important increase in the resistance and clearly identifies the core-switching field H_{sw}. When the field is further increased, the annihilation occurs and corresponds to the change in the slope of the AMR curve. Similar behaviors are found for other angles when θ is kept lower than 75°.

For applied field angles very close to the perpendicular direction, $\theta>75°$, the mechanism involved during the magnetic hysteresis is slightly modified. For the nucleation, instead of the intermediate curling state with the magnetization lying mostly along the wire axis, the vortices directly enter the nanowire. The configuration with vortices of opposite chirality is conserved since this lowers the demagnetizing energy along the wire. The circular path required for the formation of the vortices appears at the wire border. The vortex core is a little away from the wire center and moves toward the wire center as the field is decreased to zero. At remanence the system is in the same configuration as in Fig. 2. When the field is reversed, the vortex cores move toward the other wire border before being expelled.

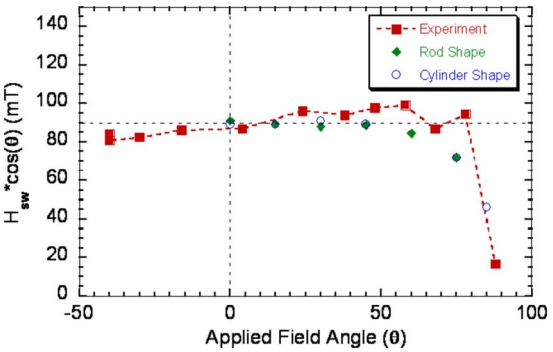

FIG. 4. (Color online) Angular dependence of the axial component of the vortex-core switching field $[H_{sw}^{z}=H_{sw}*\cos(\theta)]$ recorded in the experiments and the simulations (wire with square rod and cylindrical shapes).

Figure 4 shows the angular dependence of the vortex-core switching field (indicated by the increase in resistance between situation IV and V). In both experiments and simulations (rods and cylinder shape) the switching field evolves as $1/\cos(\theta)$, except when very close to the perpendicular direction ($\theta>75°$) where a slightly different reversal mechanism takes place. This evidences that the axial component of the applied field is responsible for the reversal of the vortices core and can be expressed, as a function of θ the applied field angle with respect to the wire axis, by

$$H_{sw}(\theta)=H_{sw}(\theta=0)/\cos(\theta) \quad (1)$$

with H_{sw}, the vortex core switching field.

When the longitudinal component of the applied field reaches the value needed to reverse the vortex core for $\theta=0$, the reversal occurs. This is also found in the simulation for both square and cylinder shapes. Even if different values for $H_{sw}(\theta=0)$ can be obtained on other geometries, this is still observed. This situation ensures a deterministic reversal law driving the irreversible part of the reversal. The volume of spins in the core lying in the opposite direction of the axial-field component has an important contribution to the Zeeman energy. This volume is large enough to determine the maximum axial-field component that the system can support before reversal begins. This appears to be a general rule of the reversal properties of the vortices in such elongated magnetic systems and gives the opportunity to geometrically control the switching field.

The simulations show that for $\theta<75°$ the core of the two vortices reverse through the nucleation of vortices with opposite core polarity, but same chirality, that propagate along the central grain area. The reversed vortices nucleate at the vicinity of the domain wall (the plane with the transverse magnetization) that separates the two original vortices. This mechanism uses a Bloch point at the front line between the cores of opposite polarity. For the 500-nm-long grain and using a 0.02 damping parameter, the reversal occurs in roughly 2 ns. In contrast to the core reversal with a Bloch point in flat-magnetic elements, this situation is observed even at large angles with respect to the polarization axis.

This study further supports the importance of Bloch points in the magnetization reversal of low-dimensional systems.

From the simulations, the nucleation and annihilation fields of the vortices appear as changes in the slope of the AMR curves. Their values can thus be extracted unambiguously from the experimental measurements. Both nucleation and annihilation fields increase with θ, showing that the vortices state is more stable when the field is applied at an angle from the wire axis. The absolute value of the annihilation field is always slightly larger (~ 10 mT) than the nucleation field. This behavior is quite different for the vortex-reversal properties in magnetic dots or rings where a large difference is observed between the nucleation and annihilation fields.

This situation is compatible with MFM observations of similar nanowires.[14] Moreover, AMR measurements either on numerous nanowires remaining in the membrane or on single and isolated nanowires, even with smaller diameters, reveal similar angular dependencies, showing that this reversal is general in such high aspect-ratio nanowires with transverse MCA. Different nanowire configurations (grain length, wire diameter, perpendicular MCA orientation) have been used in the simulations, they also show similar results. For smaller diameters, the annihilation field corresponds to the reversal of the vortex core. While the present situation has some similarities with the curling reversal, it is emphasized that the magnetization reversal starts before the field is reversed.

To conclude, we have evidenced the magnetic-vortices state in high aspect-ratio systems such as nanowires with transverse-magnetocrystalline anisotropy. Using a simple model, the micromagnetic simulations reproduce the magnetic hysteresis observed in the experiments and reveal an original vortex state. The nucleation, core reversal and annihilation are always at well-differentiable field values, so that they always occur during the magnetic hysteresis cycle. Important results come from the angular dependency of the core-switching field. It appears that the axial component of the applied field (thus antiparallel to the vortex core) determines the core-reversal field. The reversal is completely driven by the anisotropic properties and the geometry, making the magnetization reversal less sensible to the presence of defects and from sample to sample variations. This novel form of vortex state in nanowires provides the opportunity to control the switching field and to study in more detail the Bloch point singularity.

This work was partly supported by the Interuniversity Attraction Poles Program (P6/42)-Belgian State-Belgian Science Policy. L.V. thanks the CISM computation facilities of UCL.

[1] T. M. Whitney, J. S. Jiang, P. Searson, and C. Chien, Science **261**, 1316 (1993).
[2] For a review, see A. Fert and L. Piraux, J. Magn. Magn. Mater. **200**, 338 (1999), and references therein.
[3] E. C. Stoner and E. P. Wohlfarth, Philos. Trans. R. Soc. London, Ser. A **250**, 599 (1948); IEEE Trans. Magn. **27**, 3475–3518 (1991).
[4] W. F. Brown, Phys. Rev. **105**, 1479 (1957).
[5] G. P. Heydon, S. R. Hoon, A. N. Farley, S. L. Tomlinson, M. S. Valera, K. Attenborough, and W. Schwarzacher, J. Phys. D **30**, 1083 (1997).
[6] W. Wernsdorfer, B. Doudin, D. Mailly, K. Hasselbach, A. Benoit, J. Meier, J.-Ph. Ansermet, and B. Barbara, Phys. Rev. Lett. **77**, 1873 (1996).
[7] J. E. Wegrowe, D. Kelly, A. Franck, S. E. Gilbert, and J.-Ph. Ansermet, Phys. Rev. Lett. **82**, 3681 (1999).
[8] Y. Jaccard, Ph. Guittienne, D. Kelly, J.-E. Wegrowe, and J.-Ph. Ansermet, Phys. Rev. B **62**, 1141 (2000).
[9] H. Zeng, M. Zheng, R. Skomski, D. J. Sellmyer, Y. Liu, L. Menon, and S. Bandyopadhyay, J. Appl. Phys. **87**, 4718 (2000).
[10] R. Ferre, K. Ounadjela, J. M. George, L. Piraux, and S. Dubois, Phys. Rev. B **56**, 14066 (1997).
[11] M. Darques, A. Encinas, L. Vila, and L. Piraux, J. Phys. D **37**, 1411 (2004).
[12] M. Kroll, W. J. Blau, D. Grandjean, R. E. Benfield, F. Luis, P. M. Paulus, and L. J. de Jongh, J. Magn. Magn. Mater. **249**, 241 (2002).
[13] Y. Henry, K. Ounadjela, L. Piraux, S. Dubois, J. M. George, and J. L. Duvail, Eur. Phys. J. B **20**, 35 (2001).
[14] L. Vila, J. M. George, G. Faini, A. Popa, U. Ebels, K. Ounadjela, and L. Piraux, IEEE Trans. Magn. **38**, 2577 (2002).
[15] L. Belliard, J. Miltat, A. Thiaville, S. Dubois, J. L. Duvail, and L. Piraux, J. Magn. Magn. Mater. **190**, 1 (1998).
[16] L. Prejbeanu, L. Buda, U. Ebels, and K. Ounadjela, IEEE Trans. Magn. **37**, 2108 (2001).
[17] B. Van Waeyenberge, A. Puzic, H. Stoll, K. W. Chou, T. Tyliszczak, R. Hertel, M. Fähnle, H. Brückl, K. Rott, G. Reiss, I. Neudecker, D. Weiss, C. H. Back, and G. Schütz, Nature (London) **444**, 461 (2006).
[18] K. Yamada, S. Kasai, Y. Nakatani, K. Kobayashi, H. Kohno, A. Thiaville, and T. Ono, Nature Mater. **6**, 270 (2007).
[19] L. Vila, L. Piraux, J. M. George, and G. Faini, Appl. Phys. Lett. **80**, 3805 (2002).
[20] Object Oriented Micromagnetic Framework, freely available at http://math.nist.gov/oommf/.
[21] T. R. McGuire and R. I. Potter, IEEE Trans. Magn. **11**, 1018 (1975).